Adaptive Slices in Brain Haemorrhage Segmentation Based on the SLIC Algorithm

Preprint · September 2021

CITATIONS
0

READS
8

4 authors, including:

Ahmad Yahya Dawod
Chiang Mai University
19 PUBLICATIONS **80** CITATIONS
SEE PROFILE

Fangli Ying
East China University of Science and Technology
14 PUBLICATIONS **32** CITATIONS
SEE PROFILE

Adaptive Slices in Brain Haemorrhage Segmentation Based on the SLIC Algorithm

Ahmad Yahya Dawod*†,
Member, IAENG, Aniwat Phaphuangwittayakul*†, Fangli Ying†, Salita Angkurawaranon

***Abstract*—Traffic accidents have a significant impact on daily life, causing head injuries like skull fractures, brain damage, and so on. Many people fail to follow the safety regulations, such as riding a motorcycle without a helmet. The use of machine learning in brain haemorrhage research is extremely challenging since it involves the collection of patient data from computed tomography (CT) scan images. This study proposes a novel region-based segmentation approach for improving the accuracy and efficiency of CT automated 3D image processing in the analysis of brain injuries. It is quite challenging to create a highly efficient superpixel method which maintains a strategic distance from the segmentation and limited clusters of the pixels in respect to the intensity boundaries. The approach reduces computational costs, and the model achieves 97.79% accuracy in segmenting brain haemorrhage images. This study also guides the direction of future research in this domain.**

***Index Terms*—SLIC algorithm; hybrid method; thresholding; region merging; segmentation.**

I. INTRODUCTION

SEVERAL techniques are utilised for image segmentation in computer vision, from simple thresholding to sophisticated deep learning approaches with optimised algorithms. The adoption of a suitable technology depends on the aims and goals of the segmentation. In clinical application, the adoption of appropriate image segmentation techniques for medical image processing depends on factors such as the disease, complexity, bias field, etc [1]. Feature extractions and investigations in medical image processing have always been challenging, especially when employing pixel-based approaches. The most significant disadvantage of region-based techniques and histogram methods is their lack of adherence to flexibility, compactness, and boundaries. Therefore, during segmentation, the boundaries of the region under study become very blurry [2]. Since they are low in memory efficiency with high computational cost. Hence, the superpixel-based approach of segmentation using simple linear iterative clustering (SLIC) has recently been adopted and tested by various researchers and proven to be efficient and superior to the classical pixel-based-approaches in boundary preservation. To the best of the researcher's knowledge, the SLIC algorithm does not segment the 3D images of brain haemorrhages. Hence, this research is novel in its approach to the use of the SLIC algorithm to segment brain haemorrhages [3]. People who drive motorcycles do not always follow the rule of wearing a helmet for head protection and are involved in accidents on a daily basis. This research focuses on helping the doctor to make decisions concerning the patient in the early stages of diagnosis. A novel technique for brain injury CT image segmentation is proposed in this study based on superpixels, applying the following eight-step approach: 1. Input image Converting Digital Imaging and Communications in Medicine (DICOM) images into jpeg format; 2. Skull removal to clean the noise from the CT scan; 3. Pre-processing linear transformation and windowing of the images; 4. Regional merging to eliminate false boundaries; 5. Image processing using the simple linear iterative clustering (SLIC) algorithm to create superpixels; 6. Thresholding; 7. A hybrid method, combining region merging with SLIC; 8. Datasets containing 30,000 brain haemorrhage images obtained from Maharaj Nakorn Chiang Mai Hospital, Thailand.

Manuscript received June 04, 2020; revised August 17, 2020. This work was fully supported in part by International College of Digital Innovation (ICDI), Chiang Mai University, and Faculty of Medicine, Chiang Mai University, grant no. 143-2562.

Ahmad Yahya Dawod is a Lecturer at International College of Digital Innovation, Chiang Mai University, Chiang Mai 50200, Thailand (corresponding author phone: +66 650066958; e-mail:ahmadyahyadawod.a@cmu.ac.th).

Aniwat Phaphuangwittayakul is a Lecturer at International College of Digital Innovation, Chiang Mai University, Chiang Mai 50200, Thailand (corresponding author phone: +66 894346796; e-mail: aniwat.ph@cmu.ac.th).

Fangli Ying is a Lecturer at Department of Computer Science and Engineering East China University of Science and Technology, Shanghai, 200237, China; (e-mail: yfangli@ecust.edu.cn).

Salita Angkurawaranon is a Lecturer at Department of Radiology, Faculty of Medicine Chiang Mai University, Chiang Mai 50200, Thailand (e-mail: salita.ang@cmu.ac.th).

* Corresponding author.

† These authors contributed equally to this paper.

II. RELATED WORK

Researchers and practitioners have widely adopted SLIC superpixels, first introduced by [4] for pre-processing image segmentation, and their suitability for medical image processing extensively assessed. The SLIC algorithm in medical image processing [5] shows better robustness and accuracy in fuzzy boundary and segmentation [6]. Superpixel brain segmentation for tumour detection was used by [7] and the SLIC algorithm was found to improve accuracy and reduce computation time. The existing literature is replete with SLIC superpixel approaches for 2D image processing, but there is limited research on 3D image processing using the SLIC superpixels approach. [8] medical image processing is facing various challenges region's growing processing for selection automates seeds for the step of histogram threshold. Region merging is iterative since it compares all unallocated neighbouring pixels to the seeds. The difference between the regions and pixel intensity values indicates similarities with achieving high accuracy. A super-voxel technique was used by [9] for image processing in 3D space, earning a high boundary recall on 2D images, while proposed a four-stage SP generation algorithm with convexity as the

metric. Automated super-voxel segmentation was proclaimed by [10] for the extraction and reporting of geometric and statistical features. Whereas [11] developed a 3D Region of Interest based volumetric medical image retrieval using a superpixel algorithm, visualised through a web-interface. From the above works, it is clear that researchers have widely adopted the SLIC approach to 3D image processing due to its flexibility in applying multiple dimensions [12] .

III. Input Data

A dataset consisting of 3D computed tomography (CT) patient brain scans, involving more than 30000 labelled slices (IPH, EDH, SDH, MLS, IVH). The dataset was obtained from specialist doctors at the Maharaj Nakorn Chiang Mai Hospital, Thailand. Standard Digital Imaging and Communications in Medicine (DICOM) axial slices were converted into JPEG images. In this study, the proposed method for treating brain haemorrhages was evaluated using different classifier images consisting of more than 5000 slices. Slice thickness was constant in most of the 300 patient datasets with slices varying in thickness between male and female patients aged between 24 and 53 years. The chosen slice thickness is 1.5 mm for each case of the 100-150 slices. Illustration 2D shows the selected slices composed in a 3D CT brain scan sample. The first greyscale is so compressed that a small variation in intensity could be visualised inside the human skull, which is unsatisfactory. A CT scan image can ordinarily overcome this difficulty by providing a modified greyscale.

IV. Proposed Method

Eight-steps method with a novel region-based segmentation approach for improving the accuracy and efficiency of Automated 3D image processing of Computed Tomography (CT) in analyzing brain injuries is depicted in Fig. 1.

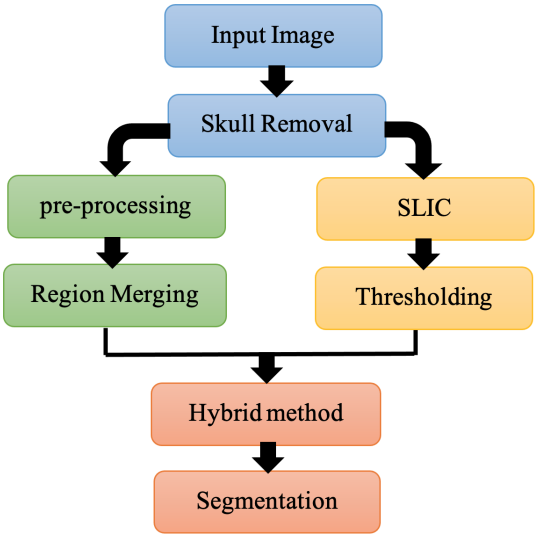

Fig. 1. Illustration of the proposed method.

A. Input Image

In the first step of the input image, more than 30,000 3D DICOM format brain images were converted into 2D JPEG format with a spatial resolution of 512×512, slice thickness of 1.5 mm, and a distance between each slice of 0.5 mm. An illustrative sample CT scan of brain slices after pre-processing and converting 3D to 2D is presented in Fig. 2. To visualise the CT scan images, the Hounsfield Units (HU) to greyscale conversion is used with a window width equal to 150 and a window level of 30 as recommended by the doctor. The slices shown in the image are linearly transformed after intensity windowing.

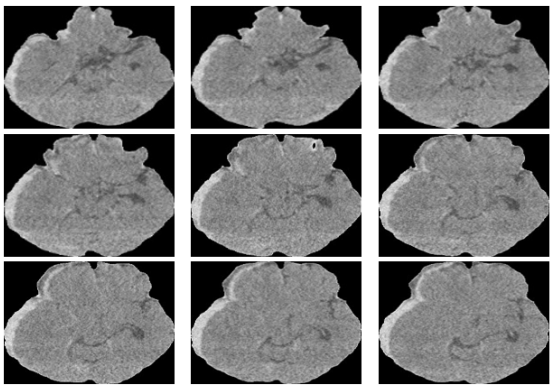

Fig. 2. Samples of CT brain slices (after pre-processing step from 3D to 2D)

B. Skull Removal

This research aims to improve the automatic skull removal method of noisy CT brain images. The skull region is removed by cropping the brain with the largest component [13]. In addition, the intensity skull and headrest are also removed to reduce computational complexity by increasing the weight of the image to improve efficiency. This illustrates the potential of clean skull removal without influencing the brain, in a significant number of CT brain images from different sources. After removal, the majority contain brain matter and lower the intensity of information the brain as shown in Fig. 3. The edge detection is applied for removing the noise of edge in the pre-processing step. The edge of brain after skull removal is drawn as Fig. 4.a.

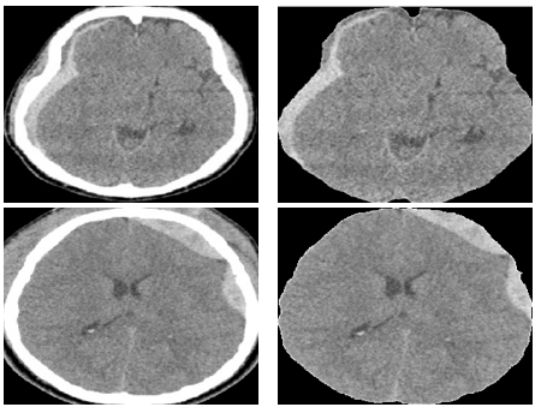

a) (b)

Fig. 3. Skulls remove for the shape of the brain. a) Before removing the skull, b) After removing the skull.

C. Pre-processing

Pre-processing is the most significant step in the proposed method. The input image intensity was linearly transformed using windowing and contrast adjustment techniques. The input image modulates the window to contrast the values depending on the ROI. The desired window intensity was adopted from the DICOM header information already provided. Equation 1 describes the linear transformation of images [14].

$$HU = (PV^* R_s) + R_i \tag{1}$$

where, HU, PV, R_s, and R_i,stand for Houndsfield unit, raw pixel value, rescale gradient, and rescale intercept, respectively. The tissue of interest in CT scans for brain haemorrhages is based on HU values [15]. The skull, calcified regions, soft tissues, cerebral spinal fluid (CSF), and haemorrhaging blood will have different HU values. Within the ROI, the haemorrhage blood has greater HU values than the soft tissues and CSF. The original HU scale of skull removal images were used as the input in this step. The hounsfield values between 60 to 85 were therefore selected to coincide with those of the brain haemorrhage, white matter and grey matter. The Hounsfield units scale image was converted into greyscale by setting the window width to 151 and the window level to 114. The HU to greyscale conversion can be calculated as Equation 2.

$$S_w(a,b) = \begin{cases} 0, & S(a,b) \le L - \frac{W}{2} \\ \frac{S(a,b)-(L-\frac{W}{2})}{W} I_{\max}, & L - \frac{W}{2} < S(a,b) \le L + \frac{W}{2} \\ I_{\max}, & S(a,b) > L + \frac{W}{2} \end{cases} \tag{2}$$

Where (W) is window width and (L) is the window level for $I_{\max} = 255$; in principle, the process draws the unique intensity scale between $(L - \frac{W}{2}, L + \frac{W}{2})$ to the highest scale of the exhibited tool. The white matter and grey inside the brain are clearly visible. The output image of HU to greyscale conversion is presented in Fig. 4.b. The noise of the output image is eliminated by the edge of skull removal brain as shown in Fig. 4.c.

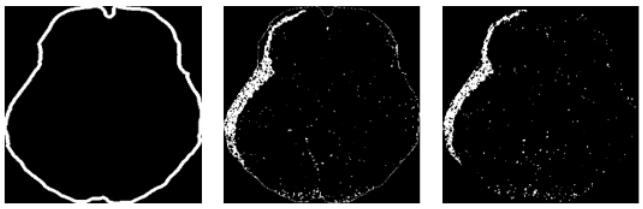

(a) (b) (c)

Fig. 4. Skulls remove for the shape of the brain. a) Before removing the skull, b) After removing the skull, c) Reduce the noise from the shape .

D. Region merging

The fourth step in the proposed approach is to merge the regions [16]. The automated seed point technique in region merging operates until no more pixels can be added to eliminate spurious regions and false boundaries while merging the haemorrhage sections. Furthermore, 3-D flood-based watershed transformation is applied to analyse brain haemorrhage intensity. The shapes with noise before use filter step are shown in Fig. 5.a, then follow the region merging results in Fig. 5.b, with the size of haemorrhage region then expanded using a 9×9 kernel matrix of dilation as shown in Fig. 5.c.

(a) (b) (c)

Fig. 5. three steps for region merging, a) Image with noise, b) Region growing, c) Thresholding result.

E. SLIC

The SLIC technique, proven to be more efficient in terms of computational power and memory usage, was used for superpixel creation and image partition [17]. If a and b are considered as pixel location coordinates with the user-specified grid size (s), the greyspace distance (d_c), and the Euclidean distance(d_s) between the j^{th} pixel and i^{th} pixel are calculated

$$d_s = \sqrt{(a_i - a_j)^2 + (b_j - b_i)^2} \tag{3}$$

With normalized intensity values (N) of the $j^{th}(N_j)$ and $i^{th}(N_i)$ pixels, the intensity distance (d_c) between the j^{th} and i^{th} pixels will be calculated as;

$$d_c = \sqrt{(N_j - N_i)^2} \tag{4}$$

S is Parameter of local clustering M, The Images Numbers, and K Superpixels Number is calculated by

$$S = \sqrt{M/K} \tag{5}$$

If compactness coefficient is p and initial super-pixel grid size is S,p balance between d_s and d_c then the overall distance D is calculated as;

$$D = \sqrt{d_s^2 + \left(\frac{d_s}{S}\right) p^2} \tag{6}$$

While application, to confirm that both the space distances and intensity are within the same range and to obtain an optimum compactness coefficient, the CT image intensities used in equation 6, are normalized to the values of [0, 1]. A sample pre-processed JPG image of a CT Scan with grade II haemorrhage in Fig. 6 shows a sample pre-processed JPG image of a CT scan with a grade II haemorrhage and super-pixelised image with a compactness factor p of 0.1 and a grid size (S) of 10. A higher value of the compactness coefficient was found to create more flexible boundaries, while a smaller value results in more compact segments Fig. 6.a. After achieving the SLIC image, the greyscale image is provided using the SLIC algorithm shown in Fig. 6.b. The results of the SLIC are shown in Fig. 6.c. The results of segmentation on a particular brain image with the initialised parameters were provided using the superpixel method. The function without the initialising requirement to create the

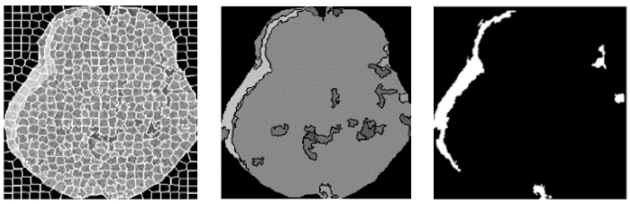

(a) (b) (c)

Fig. 6. CT image: a) The superpixels, b) RAG grayscale output, c) Result of SLIC Algorithm.

number of superpixels is convenient for each iterate type process, since it saves the computational cost of distributing memory for all structures of the procedure.

F. Thresholding

The region adjacency graph (RAG) was applied to merge the thresholding technique with pixel numbers > 160 to detect the haemorrhage. Fig. 7.a presents samples of one haemorrhage feature, while and two haemorrhage features are illustrated in Fig. 7.b. The choice of an ideal threshold

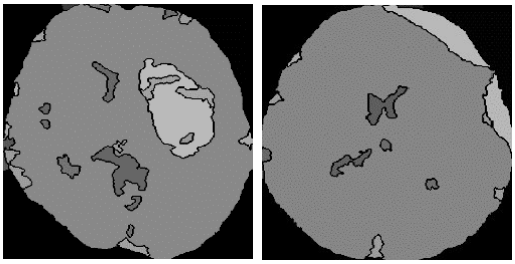

(a) (b)

Fig. 7. The process of thresholding image, a) One feature haemorrhage, b) Two feature haemorrhage.

value provides a more outstanding image threshold operation. The mean and variance are used to measure the described images. When the final threshold is reached, each pixel of image $g(i,j)$ is related to T. Pixels higher than T are measured as edge pixels which be white shape otherwise, it is presented as black region(0). The clustering image $\int(i,j)$, can be estimated.

$$\int(i,j)\left\{\begin{array}{ll} 1 & g(i,j) \geq T \\ 0 & \text{otherwise} \end{array}\right\} \tag{7}$$

Pixel at (i,j) takes possession of $g(i,j)$ smaller than T, which is a background pixel; otherwise, it is an edge pixel. The Clustering with value as (1) which use for white shape and pixels clustering with value as (0) is non-pixels showing the background [18].

G. Hybrid Method

In this section, a more challenging hybrid technique is presented to improve the analysis results by providing bitwise operation between two outputs to correlate the region of haemorrhage between the SLIC algorithm and the region merging method following equation 8.

$$C = A \otimes B \tag{8}$$

Algorithm 1 Thresholding Algorithm

Require: Original image a is Initialize, The mean of a (M) is the number , The variance of a (V) is the number
Initialization Step
InjuryCode for Threshold()
if $(1.9 \leq \frac{M}{V} \leq 1.8 \| 1.5 \leq \frac{M}{V} \leq 1.7)$ **then**
    Set threshold $T = 160$
else
    Set threshold $T = 170$
end if
if value means of the pixel intensity of region $< T$ **then**
    Not injury of the region
else
    Have injury for the region
end if

Where A represents the SLIC result and B the output of the region merging method. Fig. 8 shows a combination of methods. Firstly, the region merging method is shown in Fig. 8.a, while the SLIC method using different stages is presented in Fig. 8.b. Finally, high-performance results are achieved using a hybrid approach as shown in Fig. 8.c.

(a) (b) (c)

Fig. 8. The processing to combine the result. a) Region merging development, b) SLIC result, c) The result of a hybrid technique.

H. Segmentation

To consider each brain image CT scan in the region and whether a pixel can be classified as a haemorrhage or non-haemorrhage, the region-based segmentation approach was used with the red pixels representing the boundary region detection cluster. In order for the central pixel to be symmetrical, the smallest matrix should be 3×3 [19]. To clearly detect the haemorrhage region, the threshold algorithm was implemented using segments with different grayscales. To provide white pixels, the haemorrhage region is segmented, and the boundary of the region detected as red pixels. The white clustering districts were filled inside the boundary. The size of the matrix in the region containing the highest number of pixels must not be outside the boundary. The ultimate result in Fig. 9.b. shows the bleeding clearly without any noise. In this research, the regional based segmentation method was used to improve segmentation performance, based on the SLIC algorithm without noise and different processing steps as shown in Fig. 10.

V. EXPERIMENTAL RESULTS

The experiments on the collected dataset have previously been discussed. The significant advantage of the proposed approach is that it achieves high classification accuracy with

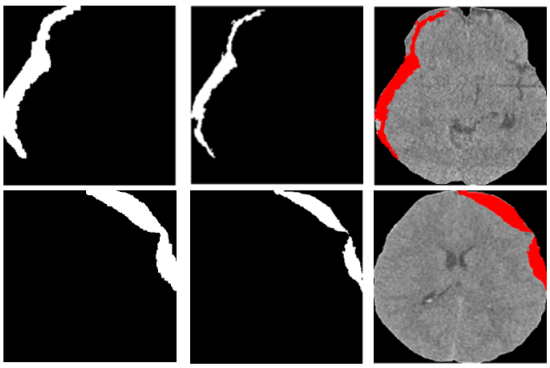

(a) (b) (c)

Fig. 9. The region haemorrhage segmentation, a) Region merging, b) A hybrid technique, c) Segmentation.

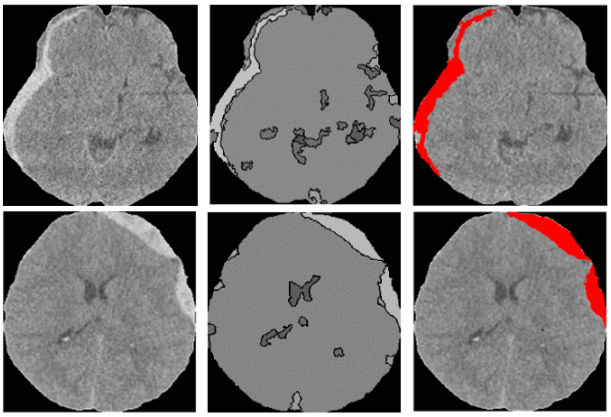

(a) (b) (c)

Fig. 10. The bleeding for the original image without the skull. a) Original image, b) Thresholding, c) Haemorrhage Segmentation.

low computational effort. The hybrid technique performs well in extracting the complex texture of a brain haemorrhage. Furthermore, the spectral clustering of this method with global eigen decomposition achieved high accuracy in segmenting the regions and sophisticated features of a brain haemorrhage. Hence, the proposed method outperforms the conventional segmentation technique for CT brain scans. It also overcomes the dense similarity construction of spectral clustering following application of the region-based segmentation model.

VI. EVALUATION METRICS AND DISCUSSION

In this study, ICH is referred to intracranial haemorrhage which consists of EDH,SDH, and IPH haemorrhage subtypes. the following thresholding and SLIC Algorithm were performed on the ICH slices, which range thresholding technique with pixel number > 160 to detect the haemorrhage and also we modify the SLIC Algorithm for Hybrid technique is presented . In this section, the performance of the proposed method is discussed by calculating the different evaluation matrices.

PPV: Also known as precision, represents the number of correct positive results divided by the number of positive consequences predicted by the classifier [20].

$$PPV = \frac{TP}{TP + FP} \times 100\% \tag{9}$$

TPR: Also known as sensitivity or recall, represents the number of correct positive results divided by the number of relevant samples.

$$TPR = \frac{TP}{TP + FN} \times 100\% \tag{10}$$

TNR: Also known as specificity, is used to measure the rate of true negatives.

$$TNR = \frac{TN}{TN + FP} \times 100\% \tag{11}$$

F_1Score: This is the harmonic mean between precision and recall. These two measures are sometimes used together in the F_1 Score (or-f-measure) to provide a single measurement for the system.

$$F_1 = \frac{2TP}{2TP + FP + FN} \times 100\% \tag{12}$$

ACC: This is a statistical measurement method, characterising how close the predictions are to the valid values [21].

$$ACC = \frac{TP + TN}{TP + TN + FP + FN} \times 100\% \tag{13}$$

Where TP is the true positive (complementary issue of the correct segment), TN is the true negative (negative point of the appropriate segment), while FP is false positive (incorrectly segmented in the complementary case), and FN is false negative (negative effect of an incorrect segment) [22].

DSC Dice Similarity Coefficient, using S stands for Segmentation, is observed from the equation 14. DSC is a tool for measuring the similarity between predicated segmentation and ground truth. Both false alarm and true positive are considered in DSC. DSC not only evaluate the accuracy of image segmentation results but also identify the correct labelled region [23] defined as.

$$DSC = \frac{2\left|S_{ICH} \cap S_{IC\hat{H}}\right|}{\left|S_{ICH}\right| + \left|S_{IC\hat{H}}\right|} = \frac{2 \times TP}{2 \times TP + FP + FN} \tag{14}$$

Jaccard Similarity Index JSI is additionally identified as Intersection-Over-Union IoU and is characterized as the ratio of the region of the similarity between the ground truth (S_{ICH}) and the predicted segmentation ($S_{IC\hat{H}}$) to the area of union between and the ground truth segmentation and the predicted segmentation.

$$JSI = \frac{S_{ICH} \cap S_{IC\hat{H}}}{S_{ICH} \cup S_{IC\hat{H}}} = \frac{TP}{TP + FP + FN} \tag{15}$$

JSI is another tool for evaluating the similarity and diversity of two datasets. The correlation of data can be calculated by JSI as equation 15. However, JSI will give more weight to incorrect results compared to DSC can be seen from the equation 16.

$$JSI = \frac{DSC}{2 - DSC} DSC = \frac{2 \times JSI}{1 + JSI} \tag{16}$$

To evaluate the measurement of the three features of a brain haemorrhage, namely EDH, SDH, and IPH segmented by different steps such as 30 to 81 slices, the

TABLE I
THE PERFORMANCE OF DIFFERENT FEATURES HAEMORRHAGE IS START FROM SLICE 30.

	Precision	Recall	F1	ACC
EDH	98.42	90.35	94.68	90.45
SDH	97.55	88.85	92.86	87.45
IPH	94.59	96.32	95.65	94.11
Average	97.76	90.33	93.90	89.34

performance of this method is accurate as shown in Table I, and average for the haemorrhage steps.

In calculating the three features of a brain haemorrhage (EDH, SDH, and IPH) segmented by various slicing steps such as 40 to 95 slices, the performance score of this approach is accurate and average for the haemorrhage stages as shown in Table II.

TABLE II
THE PERFORMANCE OF VARIOUS FEATURES HAEMORRHAGE IS BEGIN FROM SLICE 40.

	Precision	Recall	F1	ACC
EDH	99.42	90.55	94.78	97.76
SDH	97.34	88.90	92.93	98.26
IPH	97.76	97.22	95.89	97.35
Average	98.17	92.04	94.53	97.79

Therefore, the proposed technique for brain haemorrhage segmentation is compared using ten cross-validation to evaluate the estimated performance of the projection profile method. The dataset was divided into 80% training and 20% testing. Intracranial haemorrhage was analysed using CT scans by radiologists to identify ICH and focus on its regions [27].

TABLE III
THE COPMERISM BETWEEN FOUR METHODS BY USING KAGGLE.

Methods	PPV	TPR	TNR	F1	ACC
Projection Profile [24]	88.23	75.75	90.16	81.9	83
ICH UNet [25]	90	49.72	47.37	64.06	49.5
UNet++ [26]	55.56	100	0	71.42	55.56
Our Method	88.89	81.63	89.9	85.1	85.78

For regional segmentation of the ICH in a fully automated manner, the Kaggle dataset (https://www.kaggle.com/felipekitamura/head-ct-haemorrhage) consisting of 100 images with and without haemorrhage was evaluated using the four methods shown in Table III. The proposed method in this study which includes different statistical parameters was found to outperform the baseline approaches. The results can be compared using the PhysioNet dataset (https://physionet.org/content/ct-ich/1.2.0/), consisting of 318 images with haemorrhage and 340 images without haemorrhage as shown in Table IV.

The four methods were compared using the dataset in this study and different statistical measurement parameters, as indicated in Table V. The proposed technique was improved to achieve a higher performance in comparison to other methods.

The ICH sub-type showed that our method performed the best with a Dice Similarity Coefficient for the segmentation

TABLE IV
THE COMPARISON BETWEEN FOUR METHODS BY USING PHYSIONET DATASET.

Method	PPV	TPR	TNR	F1	ACC
Projection profile[24]	82.90	77.43	79.6	80.05	78.53
ICH UNet [25]	96.23	12.05	95.64	21.42	20.22
UNet++ [26]	57.64	98.43	32.35	72.71	64.28
Our Method	83.67	78.93	85.59	81.22	82.37

TABLE V
THE COMPARISON BETWEEN FOUR METHODS BY USING OUR DATASET.

Method	PPV	TPR	TNR	F1	ACC
Projection profile [24]	65.35	69.44	91.85	67.3	87.77
ICH UNet [25]	78.76	87.32	82.82	45.59	74.71
UNet++ [26]	84.88	96.44	72.14	90.29	82.50
Our Method	97.77	90.34	93.91	79.44	89.34

by users based on the 512×512 mask of the CT slices resulted. By using the ground truth segmentation from the PhysioNet dataset, we can calculate Dice Similarity Coefficient DSC and the Jaccard Similarity Index JSI of the ICH high sensitivity and segmentation is identifying the ICH regions to be respected as the following table VI.

TABLE VI
THE COMPARISON BETWEEN TWO METHODS OUR METHOD AND UNET++ BY USING JSI AND DSC

Method	Jaccard Similarity Index	Dice Similarity
ICH UNet [25]	0.22	0.31
UNet++ [26]	0.88	0.19
Our Method	0.43	0.44

We used five samples of output image to comparison between two methods our method and UNet++ method by involving Jaccard Similarity Index and the Dice score for showing on the high value for two measurements show on table VII.

TABLE VII
THE COMPARISON BETWEEN FIVE IMAGE WITH OUR METHOD AND UNET++ METHOD BY USING JACCARD SIMILARITY INDEX AND DICE SIMILARITY.

Symbols	Jaccard Similarity Index		Dice Similarity	
	Our Method	UNet++	Our Method	UNet++
A	0.71	0.44	0.83	0.63
B	0.49	0.43	0.66	0.62
C	0.81	0.79	0.88	0.89
D	0.62	0.71	0.77	0.81
E	0.49	0.43	0.66	0.62

The boundary impact of each predicted 512×512 mask was minimal. The non-ICH regions are the value of low probabilities and then converted to zero after thresholding. The final segmented ICH regions after merging the windows, thresholding, and performing for a few CT slices are presented in Fig. 11.a, demonstrates the results between ground truth (green color) and our method (red color), our model matches most of the ICH segmentation region labelled by radiologist. Fig. 11.b, presents the results between ground truth (green color) and UNet++ (blue color), there are some false-positive regions and noise regions in the output contours from UNet++.

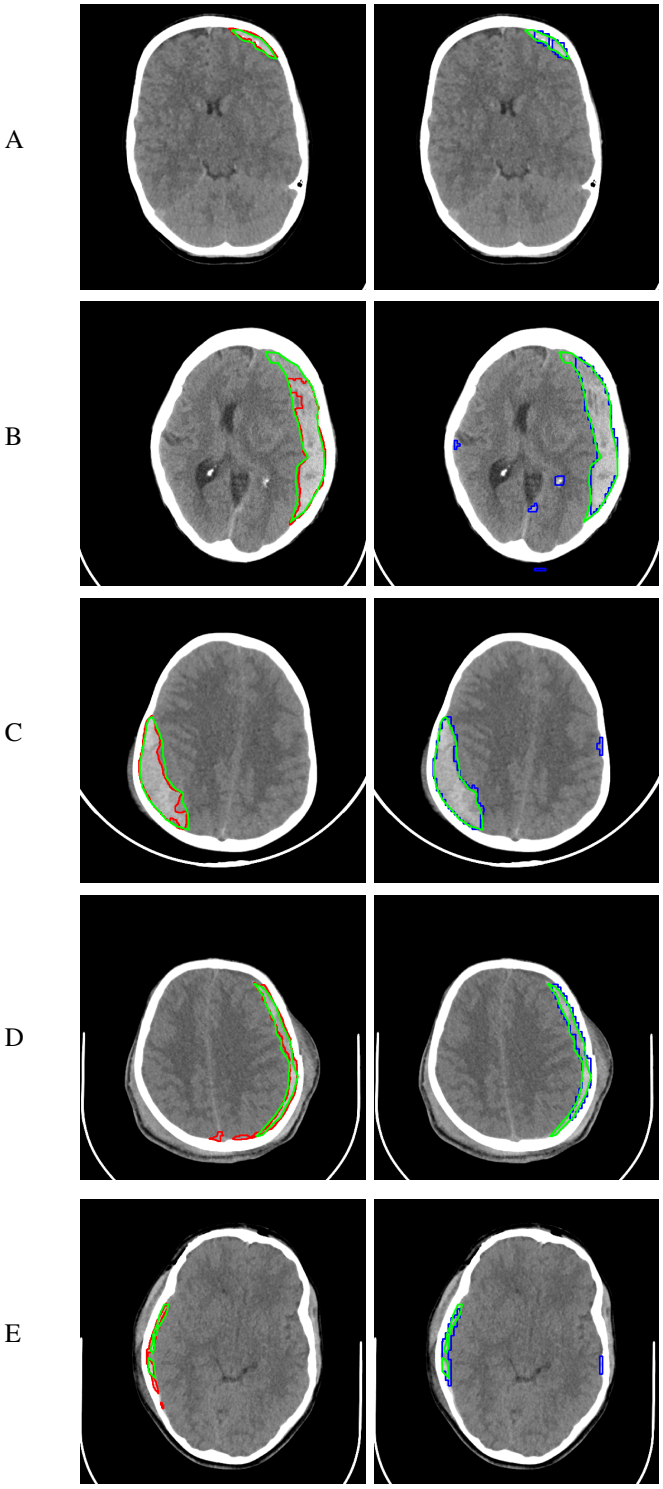

Fig. 11. The testing CT slices along with the radiologist delineation of the ICH. a) The green color is ground truth, the red color is contour from our method, b) The green color is ground truth, the blue color is contour from UNet++ method.

For evaluation purposes, the brain-injured haemorrhage considers two or three features (EDH, SDH or IPH), depending on numerous markers such as the size and location of each feature. To achieve high accuracy for different slices, the proposed method depends on reaching high-performance segmentation with fewer area errors, as show in Table VIII.

TABLE VIII
ESTIMATION OF HAEMORRHAGE INDEX FOR EDGE DETECTION ALGORITHM DIFFERENT SLICES.

Slices	Error Area	Image haemorrhage
61	1.3	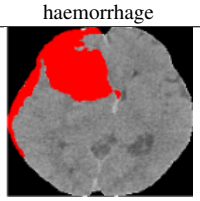
62	1.1	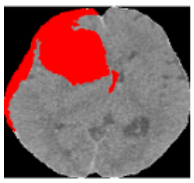
63	1.7	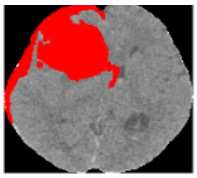
64	1.9	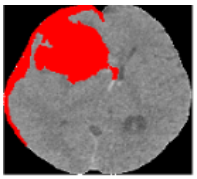
65	1.8	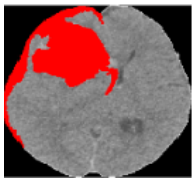
66	1.5	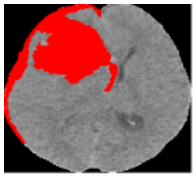

VII. CONCLUSION AND FUTURE WORK

Medical image processing of brain haemorrhages is significant in assisting specialists to diagnose an injury. In this paper, a novel regional SLIC based method is proposed, based on the superpixel technique for segmenting haemorrhages in brain scans. The images are computed using SLIC to project the boundaries in the initial step as well as segments with different greyscales. The pre-processing techniques of noise reduction and the removal of unwanted regions from brain tissue. Preliminary results of the images from the dataset used in this study indicate that the current approach of region-based and brain haemorrhage segmentation can achieve 97% accuracy. Different datasets with varying statistical measurement parameters were used to achieve different results.

REFERENCES

[1] X. W. Gao, R. Rui , and Z. Tian, “Classification of CT brain images based on deep learning networks,” Computer Methods and Programs in Biomedicine, vol. 138, pp49-56, 2017.

[2] B. Peng, L. Zhang, and D. Zhang, "A Survey of Graph Theoretical Approaches to Image Segmentation," Pattern Recognition, vol. 46, no. 3, pp1020-1038, 2013.
[3] P.E. Adjei, H. Nunoo-Mensah, R.J.A Agbesi, and J. Ndjanzoue, "Brain tumor Segmentation using SLIC Superpixels and Optimized Thresholding Algorithm," International Journal of Computer Applications, vol. 181, no. 20, pp1-5, 2018.
[4] K. Kamnitsas, C. Ledig, V.F. Newcombe, J.P. Simpson, A.D. Kane, D.K. Menon, and B. Glocker, "Efficient multi-scale 3D CNN with fully connected CRF for accurate brain lesion segmentation," Medical Image Analysis, vol. 36, pp61-78, 2017.
[5] J. Cong, B. Wei, X. Xi, Y. Zheng, and Y. Yin, "Performance evaluation of simple linear iterative clustering algorithm on medical image processing," Bio-Medical Mater, vol. 24, no. 6, pp3231-3238, 2014.
[6] Q. Zhang, M. Yang, K. Kpalma, Q. Zheng, and X. Zhang, "Segmentation of hand posture against complex backgrounds based on saliency and skin colour detection," IAENG International Journal of Computer Science, vol. 45, no. 3, pp435-444, 2018.
[7] M. Soltaninejad, G. Yang, T. Lambrou, N. Allinson, T. L. Jones, T. R. Barrick, F. A. Howe, and X. Ye, " Automated brain tumour detection and segmentation using superpixel-based extremely randomized trees in FLAIR MRI," International Journal of Computer Assisted Radiology and Surgery, vol. 12, no. 2, pp183-203, 2016.
[8] M. Saad, S.A.R. Abu-Bakar, S. Muda, M. Mokji, and A.R. Abdullah, "Fully Automated Region Growing Segmentation of Brain Lesion in Diffusion-weighted MRI," IAENG International Journal of Computer Science, vol. 39, no. 2, pp155-164, 2012.
[9] Y. Zhou, L. Ju, and S. Wang, "Multiscale superpixels and supervoxels based on hierarchical edge-weighted centroidal voronoi tessellation," IEEE Transactions on Image Processing, vol. 24, no. 11, pp3834-3845, 2015.
[10] E. Tasli, C. Cigla, and A. Alatan, "Convexity constrained efficient superpixel and supervoxel extraction," Signal Processing: Image Communication, vol. 33, pp71-85, 2015.
[11] B. Andres, U. Koethe, T. Kroeger, M. Helmstaedter, K. L. Briggman, W. Denk, and F. A. Hamprecht, "3D segmentation of SBFSEM images of neuropil by a graphical model over supervoxel boundaries," Medical Image Analysis, vol. 16, no. 4, pp796-805, 2012.
[12] A. Foncubierta-Rodrńiguez, H. Muller, and A. Depeursinge, "Region-based volumetric medical image retrieval," Progress in Biomedical Optics and Imaging - Proceedings of SPIE, vol. 8674, p867406, 2013.
[13] B. Shahangian, and H. Pourghassem, "Automatic brain hemorrhage segmentation and classification algorithm based on weighted grayscale histogram feature in a hierarchical classification structure," Biocybernetics and Biomedical Engineering, vol. 36, no. 1, pp217-232, 2016.
[14] A. Bakkari, and A. Fabijańska, "Features Determination from Super-Voxels Obtained with Relative Linear Interactive Clustering," Image Processing& Communications, vol. 21, no. 3, pp69-79, 2016.
[15] W.D. Zech, C. Jackowski, Y. Buetikofer and L. Kara, "Characterization and differentiation of body fluids, putrefaction fluid, and blood using Hounsfield unit in postmortem CT," International Journal of legal medicine, vol. 128, no. 5, pp795-802, 2014.
[16] Y. Wu, Z. Zhao, W. Wu, Y. Lin, and M. Wang, "Automatic glioma segmentation based on adaptive Superpixel," BMC Medical Imaging, vol. 19, no. 1, pp1-14, 2019.
[17] X. Wang, P. Ma, and J. Zhao, "Brain tumor CT image segmentation based on SLIC0 superpixels," International Congress on Image and Signal Processing, Biomedical Engineering and Informatics IEEE, pp427-431, 2016.
[18] M.S. Chaibou, PH. Conze, K. Kalti, B. Solaiman, and M.A. Mahjoub, "Adaptive strategy for superpixel-based region-growing image segmentation," Journal of Electronic Imaging, vol. 26, no. 6, pp1-24, 2017.
[19] A. Irimia, A. S. Maher, K. A. Rostowsky, Chowdhury, N. F. Hwang, D. H. and Law, E. M, "Brain segmentation from computed tomography of healthy aging and geriatric concussion at variable spatial resolutions," Frontiers in Neuroinformatics, vol. 13, no. 9, pp1-12, 2019.
[20] M. Koeshardianto, E. M. Yuniarno, and M. Hariadi, "Automatic Matting Using Edge Feature-Based Scribbles," IAENG International Journal of Computer Science, vol. 46, no. 3, pp459-466, 2019.
[21] AY. Dawod, J. Abdullah, and M.J. Alam, "A New Method for Hand Segmentation Using Free-form Skin Color Model," International Conference on Advanced Computer Theory and Engineering, Cybetjaya, Malaysia, vol. 2, pp562-566, 2010.
[22] A. Dehzangi, R. Hefterman, A. Sharma, J. Lyons, K. K. Paliwal, and A. Sattar, "Gram-positive and Gram-negative protein subcellular localization by incorporating evolutionary-based descriptors into Chou's general PseAAC," Journal of Theoretical Biology, vol. 364, pp284-294, 2015.
[23] I. R. I. Haque, and J. Neubert, "Deep learning approaches to biomedical image segmentation," Informatics in Medicine Unlocked, vol. 18, p100297, 2020.
[24] S. Thay, P. Aimmanee, B. Uyyanavara, and P. Rukskul, "Fast Hemorrhage Detection in Brain CT Scan Slices Using Projection Profile Based Decision Tree," In Proceedings of the 2018 International Conference on Intelligent Information Technology, pp18-21, 2018.
[25] M. D. Hssayeni, M.S. Croock, A.D. Salman, H.F. Al-khafaji, Z.A. Yahya, and B. Ghoraani, "Intracranial Hemorrhage Segmentation Using A Deep Convolutional Model," Data, vol. 5, no. 1, pp1-18, 2020.
[26] N. H. Rajini, and R. Bhavani, "Computer aided detection of ischemic stroke using segmentation and texture features," Measurement, vol. 46, no. 6, pp1865-1874, 2013.
[27] J. Cho, I. Choi, J. Kim, S. Jeong, Y.S. Lee, J. Park, and M. Lee," Affinity Graph Based End-to-End Deep Convolutional Networks for CT Hemorrhage Segmentation," International Conference on Neural Information Processing, pp546-555, 2019.

Ahmad Yahya Dawod received his Bachelor degree from the Faculty of Computer Science at Al-Mustansiriya University, Iraq in 2006. He finished his Master degree from Faculty of Computing and informatics at Multimedia University - MMU Cyberjaya, Malaysia in 2012. He finished his Ph.D. from the Faculty of information science and technology at National university of Malaysia in 2018. He is Currently as lecturer at International College of Digital Innovation Chiang Mai University, Chiang Mai, Thailand. His research interests include image processing, Artificial Intelligent, machine learning, pattern recognition, and medical image analysis.

Aniwat Phaphuangwittayakul received B.Eng. from the Faculty of Computer Engineering, Chiang Mai University, Thailand, in 2012, and Master of Science from Beijing Institute of Technology, Beijing, China, in 2017. He is currently a Lecturer in the International College of Digital Innovation, Chiang Mai University as well as a Ph.D. candidate in East China University of Science and Technology, China. His current research interests are Meta-Learning, Deep Generative Model, Computer Vision and Artificial Intelligence.

Fangli Ying received the B.S. degree from the Department of Software Engineering, Zhejiang University, Hangzhou, China, in 2009, and the Ph.D. degree from the Department of Computer Science, National University of Ireland, Maynooth, in 2014. He is currently a Lecturer in the Department of Computer Science at East China University of Science and Technology and he is also a visiting professor in the International College of Digital Innovation at Chiang Mai University, Chiang Mai, Thailand, and works with State Key Laboratory of Bioreactor Engineering, East China University of Science and Technology, Shanghai, China. His current research interests include computer vision, GIS and IoT for bioprocessing.

Salita Angkurawaranon received her medical degree from Chiang Mai University in 2005 and finished her specialization in Radiology in 2009. She finished her fellowship is neuroradiology from Ramathibodi Hospital, Mahidol University in 2014. She is current an Assistant Professor in neuroimaging at the Department of Radiology, Faculty of Medicine, Chiang Mai University.